CHEMMEDCHEM
Chemistry & Drug Discovery

Supporting Information

Indolicidin Targets Duplex DNA: Structural and Mechanistic Insight through a Combination of Spectroscopy and Microscopy

Anirban Ghosh,[a] Rajiv Kumar Kar,[a] Jagannath Jana,[a] Abhijit Saha,[b] Batakrishna Jana,[b] Janarthanan Krishnamoorthy,[c] Dinesh Kumar,[d] Surajit Ghosh,*[b] Subhrangsu Chatterjee,*[a] and Anirban Bhunia*[a]

cmdc_201402215_sm_miscellaneous_information.pdf

Table of Content

1.1 Table and Scheme Legends

Table S1. ^{1}H Chemical shift values for all the non exchangeable and exchangeable protons for GG28.

Table S2. Distance Restraints used for NMR structure calculation of GG28

Table S3. Torsion angles and pseudo phase angle restraints used for NMR structure calculation of GG28

Table S4. The gamma (ɣ) and epsilon (ε) value of oligonucleotide in free GG28 and and GG28-IR13 complex.

Table S5. Thermodynamics parameters derived using van't Hoff equation from CD melting curve.

1.2 Figure Legends

Scheme S1: (A) Sequence of Biotin and Rhodamine labelled GG28. (B)Sequence of GC28

Figure S1: Low field region of the one-dimensional proton NMR spectra of 1 mM indolicidin (20 mM sodium phosphate buffer, pH 7.2 containing 1 mM EDTA and 50 mMNaCl) at 500 MHz and at 25℃. The line broadening of the amide peaks as well as the indole ring protons of Trp clearly indicates that the indolicidin aggregates in the solution.

Figure S2: Immobilisation of Biotin-Rhodamine DNA on biotin micropatterned surface through biotin-neutravidin-biotin interaction. Scale bar corresponds to 10 µm.

Figure S3: (a) Immobilisation of Avidin-Rhodamine dye on biotin micropatterned surface through avidin-biotin interaction. (b) No green coloured, micropatterned surface indicates that FITC-IR13 peptide did not bind with biotin micropatterned surface nonspecifically. Scale bar corresponds to 10 µm.

Figure S4: CD melting of GC28 (black colour) in the absence as well as in the presence of IR13 (red colour).

Figure S5: (A) Selected regions of NMR constrained DNA duplex structure of DNA base pairs: A5-T24; T6-A23; T9-A20 and A10-T19. MD ensemble structures of base pairs (B) T6-A23; G7-C22; (C) T6-A23; A5-T24; (D) T9-A20 and A10-T19. All the A-T base pairs are highly dynamic whereas G-C base pairs are conserved.

Figure S6: Bar diagrams summarizing imino proton relaxation parameters of the free (Red) and IR13 bound GG28 (blue). (Upper panel) (A) Longitudinal relaxation rates (R_1), (B) transverse relaxation rates (R_2). (Lower panel) Space filling model showing close proximity of (C) T6, T9, T19, T24 and (D) G7, G21of GG28 with IR13.

Figure S7: Two dimensional selected ^{1}H-^{1}H NOESY spectra of GG28 (purple) and in complex with IR13 (orange) at 500 MHz, 25℃ and at 150 ms mixing time. Both the spectra are isochronous, indicating that the backbone conformations of GG28 are not changed in the presence of IR13.

Figure S8: 1H-31P correlation spectrum of GG28, showing the correlation between 3'-5' phosphorus with H5'/H5" and H3' which leads to inform that the γ and ξ dihedral exists in + and *trans* conformations, respectively.

Figure S9: Representation of GG28-IR13 complex from different snapshots of MD simulation time scale.

Figure S10: Comparison of the helical parameters for the ensemble of ten structures obtained for control DNA duplex, GG28 and the GG28-IR13 complex. The parameters were calculated using X3DNA program.

Figure S11: Average rmsd of DNA base from 50 ns MD simulation of NMR restraint derived GG28 and GG28-IR13 complex. The bar diagram of average rmsd represents the magnitude of deviation of all DNA bases in GG28-IR13 complex with reference to GG28.

Figure S12: A diagrammatic comparison of the hydrophobic region induced by IR13 residues responsible for desolvation of nucleo-bases. All snapshot were collected after 50 ns MD simulation.

2. Materials and Methods:

DNA duplexes, GG28 [d(5'-GCGCATGCTACGCG-3')$_2$] and GC28 [d(5'-GCGCATATTAATGC-3')$_2$] were purchased from Eurofins Genomics India Pvt Ltd, Bangalore, India. HPLC pure DNA sample was dissolved in aqueous phosphate buffer (20 mM sodium phosphate, 1 mM EDTA and 50 mM NaCl) of pH 7.2 and annealed at 80 ^{o}C for 5 minutes in a water-bath, cooled down slowly to room temperature overnight. Commercially synthesized and HPLC purified indolicidin (IR13) and N-ter FITC labelled indolicidin (FITC-IR13) were purchased from GL Biochem (Shanghai, China). Indolicidin containing ^{15}N labelled Leucine (IR13-^{15}N-Leu2) and its mutant peptides (IR13AA, IR13FF and IR13HH) were synthesized in Solid phase Peptide synthesizer (Aapptec Endeavor 90) using Fmoc chemistry.[1] The peptides were purified using reverse phase HPLC system (SHIMADZU, Japan) using Phenomenix C_{18} column (dimension 250 × 10 mm, pore size 100 Å, particle size 5 µm) by linear gradient elution using dual solvent system (Water and Acetonitrile) both containing 0.1 % TFA. All other chemicals used were of reagent grade from Sigma (St. Louis, MO). Cell culture dimethyl sulfoxide (DMSO), 4, 6-diamidino-2-phenylindole (DAPI), *β*-casein, Dulbecco Modified Eagle Medium (DMEM), Kanamycin sulfate, Trypsin-EDTA solution, Sodium Chloride, Potassium Chloride and fetal bovine serum were purchased from Sigma Aldrich. 2-[4-(2-hydroxyethyl) piperazin-1-yl] ethanesulfonic acid (HEPES) was purchased from Himedia. Penicillin-Streptomycin and Neutravidin were purchased from Invitrogen. Sodium bicarbonate was purchased from Merck. Rhodamine-avidin dye was purchased from vector laboratories. Cover glass bottom dishes were purchased from SPL Life Sciences, Korea. All the materials were used without further purification. A549 (Adenocarcinomic human alveolar basal epithelial cells) cell line was purchased from NCCS, Pune (India) and cultured in our lab.

2.1 Fluorescence Spectroscopy:

All fluorescence experiments were performed using Hitachi F-7000FL spectrophotometer with 1 mm path length quartz cuvette and 5 nm slit width for excitation and emission. To monitor GG28 and IR13 binding interaction, 10 µM N-ter FITC-Labelled IR13 was titrated with an increasing concentration of GG28 up to 25 µM. All the experiments were performed in 10 µM in 20 mM sodium phosphate buffer (pH 7.2), containing 1 mM EDTA and 50 mM NaCl. FITC (5(6)-fluorescein isothiocyanate), the labelling group was excited at 485 nm and emission profile was monitored at 500-600 nm range.[2] The % enhancement of fluorescence emission intensity of FITC-IR13 was calculated using equation (1) and plotted against GG28 (concentration in µM) to calculate the equilibrium dissociation constant (K_D).

% Enhancement of fluorescence intensity= $(F-F_o)/F_o \times 100$ %.....Equation (1)

Where, F =emission intensity maxima of the FITC labelled IR13 for each successive addition of GG28, F_0=emission intensity maxima of the FITC labelled IR13 without addition of GG28. To obtain the K_d value two independent single site binding equations were used to fit each of the two phases in the resulted bi-phasic curve.

To determine whether IR13 binds to the minor groove of GG28, a minor groove binding fluorescent strain 4', 6-diamidino-2-phenylindole (DAPI), was used which binds selectively A-T rich minor grove of Duplex DNA.[3] The excitation wavelength was 372 nm and emission profile was monitored from 400-520 nm.

2.2 UV-visible Spectroscopy:

All absorbance spectra were measured on a Hitachi U-2910 double beam double monochromator spectrophotometer at 25 °C in 1 cm path length quartz cuvettes. In order to understood whether IR13 binds to the major grove of GG28, we performed UV visible spectroscopy by using a major groove binding dye methyl green.[4] Briefly, methyl green was mixed with GG28 in 1:1 molar ratio and its absorption spectrum was scanned in the range of 500 to 700 nm. The change in the absorption at the λ_{max} of the dye (632 nm) was monitored at each successive addition of peptides (IR13 and IR13AA) and plotted against peptide concentration. All the experiments were performed in 20 mM sodium phosphate buffer (pH 7.2), containing 1 mM EDTA and 50 mM NaCl.

2.3 Study of DNA-peptide interaction on biotin micropattern:

Biotin micropatterned surfaces were generated using square micropatterned photo mask and UV light.[5] A flow chamber was made using that micropatterned glass surface and poly-L-lysine (PLL)-PEG passivated counter glass and equilibrated for 7 minutes with *β*-casein solution (1 mg/mL) in HEPES buffer keeping it in ice cold metal block. To study the binding of 561-labelled DNA, GG28 (F), on the biotin micropattern, we incubated the flow chamber with neutravidin (0.3 µM) solution in HEPES buffer for 7 minutes, excess neutravidin was washed out by HEPES buffer and after that 62 µM solution of the DNA was flowed into the flow chamber and incubated for 10 min. Excess DNA was removed by washing with the HEPES buffer. Finally 20 µL solutions of those peptides (FITC-IR13, FITC-IR13AA) in HEPES buffer were loaded into the flow chamber (all the peptide concentrations were 100 µM) and incubated for 10 min. Excess peptide solution was washed out by HEPES buffer. After the termination of the experiment, Flow chambers were observed by Nikon Eclipse Ti-U inverted fluorescence microscope in 561 and 488 nm channels.

2.4 Cellular uptake of peptides:

A549 cells were cultured in Dulbecco Modified Eagle medium (DMEM) containing 10% (v/v) heat-inactivated fetal bovine serum at 37^0C and 5% CO_2 atmosphere. For cellular uptake experiment, 5000 cells were seeded onto a cover glass bottom dish, one day prior to incubation with the FITC-IR13 and FITC-IR13AA peptides. All these peptides are commercially purchased and used without further purification. All those peptides were dissolved in autoclaved water and from that peptide solution of 100 µM concentration were prepared in serum-free DMEM medium. 200 µL of solution of each peptide was treated into the cells after washing with the 1X phosphate-buffered saline (PBS) and incubated for 4 hours at 37^0C under 5% CO_2 atmosphere. The nucleus was stained with 3 µM solution of 4, 6-diamidino-2-phenylindole (DAPI) in DMEM medium having <0.1%. DMSO concentration (Stock solution was prepared in cell culture DMSO) was loaded into the cell for 1 hour. Cellular internalization of those peptides was imaged by Nikon Eclipse Ti-U inverted fluorescence microscope in 405 & 488 nm channels along with bright field.

2.5 Circular Dichroism Spectroscopy:

Circular dichroism (CD) experiments were performed in Jasco J-815 spectrometer (Jasco International Co., Ltd. Tokyo, Japan) equipped with peltier cell holder and temperature controller CDF-426 L at 25 ^{o}C. The initial concentration of DNA was 10 µM in 20 mM sodium phosphate buffer (pH 7.2), containing 1 mM EDTA and 50 mM NaCl. This is used for subsequent titration with varying concentrations of IR13 ranging from 5 to 20 µM. The samples were scanned over the range of 210 to 320 nm at a scanning speed of 100 nm.min^{-1}. Data points were taken at an interval of 1 nm, averaged over 4 repetitive scans using 2 mm path length quartz cuvette. The data obtained in milli-degree were converted to molar ellipticity (ME) (deg.cm^2.dmol^{-1}) for analysis.

CD Melting experiments were performed for GG28, GG28-IR13 and GG28-IR13AA complex at of 1:1 molar ratio using the same protocol stated above. The sample was heated from 5 to 95 ^{o}C with a heating rate of 2.5 ^{o}C. Min-1. Prior to data acquisition the sample cell was equilibrated for 5 minutes at each temperature. Cuvette-holding chamber was flushed with a constant stream of dry nitrogen gas to avoid condensation of water vapour exteriorly over cuvette at low temperature. The fraction of GG28 in duplex state was calculated using equation (2) and plotted against temperature.[6] Melting Temperature (T_m) was calculated by fitting to a sigmoidal curve assuming two state models.

$\alpha = \theta_t - \theta_s / \theta_d - \theta_s$ .....Equation (2)

where, θ_t= observed CD value in milli-degree at Temperature T, θ_d and θ_s are the observed CD values in millidegree when DNA is in fully double stranded and single stranded conformation, respectively i.e., at the starting and end temperature of the melting experiment. We used equation (3) to fit the resulted duplex fraction (α) against different temperatures (T), to obtain the melting temperature (T_m). In equation (3), a, b are adjustable fitting parameters. The thermodynamic parameters i.e., ΔH, ΔG, ΔS for the free DNA and DNA-peptide complex were calculated using van't Hoff equation (4) (Table S1) in accordance with the literature.[7]

$\alpha = a/(1+\exp(-(T-T_m)/b)$ ……..... Equation (3)

$dlnK/dT = \Delta H/RT^2$……..... Equation (4)

Where K= equilibrium constant at temp T in Kelvin, ΔH= enthalpy change for the process, R= universal gas constant.

2.6 NMR Spectroscopy:

The NMR samples were prepared in 95 % H_2O, 5 % D_2O or 99.99 % D_2O, 50 mM NaCl, 20 mM Na_2HPO_4, 1 mM EDTA, pH 7.2 with 1 mM DNA concentration and DSS (2,2-Dimethyl-2-silapentane-5-sulfonate sodium salt) as an internal chemical shift reference. All the two-dimensional NMR spectra used in this study were collected at 25 ^oC using Bruker Avance III 500 MHz (Bose Institute, Kolkata) and 800 MHz equipped with 5 mm cryoprobe (Center for Biomedical Magnetic Resonance, Lucknow) with the facility of z-pulsed field gradients and a computer-controlled variable-temperature (VT) module to regulate the temperature. The NOESY spectra were acquired at 500 and 800 MHz with a spectral width of 20 ppm either the sample containing H_2O or 99.99 % D_2O in both the t_2 and t_1 dimensions, with 2048 (ω_2) and 512 (ω_1) complex points, a saturation delay of 1.5 s. The NOESY experiments for free DNA was performed with four different mixing times, ca. 80, 100, 120 and 150 ms.
DQF-COSY spectra were acquired with a spectral width of 20 ppm in both the t2 and t1 dimensions, with 2048 (ω2) and 128 (ω1) data points and saturation delay of 2.0 s. The inverse ^1H-^{31}P-correlation spectra were measured with the delay, τ, in the INEPT step adjusted to give J_{HP} of 5 to 20 Hz, 256 scans and 256 experiments.The two-dimensional NMR data were processed by Topspin software suite (Bruker, Switzerland) and analysed using the program SPARKY (Goddard, T. D., and Kneller, D. G., University of California, San Francisco). A series of one-dimensional temperature dependent ^1H proton NMR spectra for both the free DNA duplex as well as the IR13 bound DNA at a molar ratio of DNA : IR13= 1 : 1, were recorded at 500 MHz NMR spectrometer to measure the relative thermal stability of IR13 bound DNA in comparison to the iso-sequential free DNA. The 1D spectrum was acquired using excitation sculpting scheme for water suppression. The acquisition parameters were, 20 ppm for spectral width and 128 transients, a relaxation delay of 2 s, and an acquisition delay of 1.7 s. The spectra were processed and plotted with TopSpin software suite (Bruker, Switzerland) using a line broadening factor of 1.0 Hz.
One dimensional relaxation experiments for protons namely, T_1, T_2 and $T_{1\rho}$ were performed in a 500 MHz Bruker Avance III spectrometer. The T_1 experiments were performed with the inversion recovery delays of 50 ms, 150 ms, 300 ms, and 450 ms, 600 ms, 800 ms, 1 s, 1.2 s, 1.4 s, 1.6 s, 1.8 s, 2 s, 3 s, 5 s and 7 s. The measurement for T_2 using CPMG refocusing experiments were performed with increasing delays of 1 ms, 3 ms, 7ms, 12 ms, 15 ms, 18 ms, 25 ms and 50 ms. On-resonance $T_{1\rho}$ experiments were performed at the spin-lock field strengths of 3 KHz to 6KHz. R_{ex} was estimated from the $R_{1\rho}$ value calculated at 3KHz and 6 KHz using the formulae, $R_{ex}=R_{1\rho}$ (3 KHz)-$R_{1\rho}$(6 KHz) and $R_{1\rho} = R_0+R_{ex}$, where, R_0 is the T_2 relaxation rate devoid of any contributions from the chemical exchange (K_{ex}).[8] Here we made a valid assumption that the contribution of R_{ex} is negligible at higher spinlock field (6 KHz) compared to a lower spin lock field (3 KHz).

2.7 Structure Calculations:

Three dimensional high resolution solution structure was calculated based on the NMR restrained molecular dynamics (MD) simulation. Model of DNA duplex GG28 was built using NAB from David Case Group (http://structure.usc.edu /make-na/). Leap program was used from AMBER 11[9] to read in force field (ff99SB)[10] topology and co-ordinate information to generate requisite files. A short minimization was performed with GG28 model to obtain a starting point for structure calculations with experimental restraints using sander program. On the basis of NOE cross peak intensities from ^1H-^1H 2D NOESY spectrum, NOE intensities were qualitatively categorized as strong, medium and weak and translated to the upper distance limit to 3.0, 4.0 and 5.0 Å, respectively. The lower limits were varied from 1.8 to 3.5 Å. In addition to 355 inter proton NMR restraints, 62 Watson-Crick, 28 sugar pucker and 164 backbone torsion angle restraints were used for the structure calculation (Table S2 and S3). The restrained files

were processed in AMBER using nmropt = 1 option and then minimization of the model is performed with lower and upper bound force constants of 10 kcal. mol^{-1}. A simulated annealing procedure was applied in vacuum with Generalized Born model as a final step in structure calculation. The model was heated upto 400 K for 10 ps and then it was slowly cooled to 300 K in next 10 ps and then cooled to 0 K for next 5 ps. The cycle was repeated for five times. The NMR ensembles were obtained with lowest rmsd values. Structures were visualized using Chimera, PyMOL and Maestro software and the solution structures were validated using X3 DNA software suite (http://x3dna.org/).[11]

2.8 Model of GG28 -IR13 complex:

The three dimensional structure of IR13 (PDB accession code: 1G8C)[12] was docked to the solution structure of GG28 using Hex.[13] Furthermore, the final complex structure was refined by energy minimization protocol.

2.9 Molecular Dynamic Simulation:

The NMR derived GG28 structure was used for a 50 ns MD simulation in Desmond (Desmond Molecular Dynamics System, version 3.1, D.E. Shaw Research, New York, NY, 2012. Maestro-Desmond Interoperability Tools, version 3.1, Schrödinger, New York, NY, 2012) using AMBER ff99SB force field.[10] To study the structural changes of DNA, the interacting refined model of GG28-IR13 complex was also processed for MD simulation for the same time period. Both the system were solvated in orthorhombic water-box using TIP3 water models[14] using a cut-off radius of 12 Å. For neutralization of the system, appropriate Na^+ counter ions were added in both the solvated models. The initial convergence of the system to its near minima for adjustment of solute and solvent was performed with a minimization threshold of 1.0 $kcal.mol^{-1}.Å^{-1}$. The initial relaxation and equilibration of the system prior to the production run was done using Berendsen thermostat and barostat in NPT ensemble and finally the temperature of the system was raised up to 300 K to provide velocity to counter the dynamics in periodic boundary conditions. Iso-thermal-isobaric ensemble was adopted as the micro canonical ensemble for MD simulation of both the models under study. The ensemble was processed using thermostat method and barostat method.[15] The relaxation times for thermostat and barostat methods were 1 ps and 2 ps, respectively during which the temperature and pressure of the system were maintained at 300 K and 1 atm, respectively. Smooth *Particle Mesh Ewald* (PME) was applied for the calculation of non-bonded interactions of the dynamics system.[16] *SHAKE* algorithm was implemented to freeze the vibrations of bonds involving hydrogen with an integration time step of 2 ps.[17] The trajectories were saved at an interval of 5 ps for the analysis. All figures were prepared using Pymol and Chimera visualising software.

3. Tables and Figures

Table S1. ^{1}H Chemical shift values for all the non-exchangeable and exchangeable protons for GG28.

	1'H	**2''H**	**2'H**	**3'H**	**4'H**	**H5**	**H6**	**H8**	**Me (H71/H72/H73)**	**H1**	**H61**	**H62**	**H3**	**H41**	**H42**
G1	6.19	2.71	2.58	4.95	4.38	-	-	7.74	-	-	-	-	-	-	-
C2	5.81	2.42	1.97	4.80	4.18	5.76	7.41	-	-	-	-	-	-	6.64	8.47
G3	5.99	2.78	2.64	5.00	4.38	-	-	7.98	-	13.02	-	-	-	-	-
C4	5.65	2.04	2.04	4.88	4.16	5.41	7.42	-	-	-	-	-	-	6.43	8.30
A5	6.21	2.91	2.67	5.01	4.41	-		8.31	-	-	6.30	7.60	-	-	-
T6	5.73	2.42	2.03	4.87	4.13	-	7.09	-	1.32		-	-	13.48	-	-
G7	5.86	2.82	2.64	4.97	4.37	-	-	7.81	-	12.51	13.13	13.13	-	-	-
C8	5.58	2.22	1.93	4.74	4.20	5.25	7.38	-	-	-	-	-	-	6.50	8.10
T9	5.64	2.41	2.04	4.84	4.15	-	7.28	-	1.37		-	-	13.66	-	-
A10	6.09	2.89	2.65	5.02	4.40	-		8.26	-	-	7.40	7.60	-	-	-
C11	5.57	2.32	1.95	4.81	4.15	5.27	7.27	-	-	-	-	-	-	6.55	8.18
G12	5.92	2.77	2.65	4.95	4.34	-	-	7.86	-	12.94	-	-	-	-	-
C13	6.21	2.35	1.91	4.85	4.09	5.43	7.44	-	-	-	-	-	-	6.58	8.50
G14	6.17	2.79	2.65	4.99	4.35	-	-	7.95	-		-	-	-	-	-
C15	5.76	2.38	2.00	4.87	4.18	5.27	7.42	-	-	-	-	-	-		
G16	5.95	2.77	2.64	4.99	4.37	-	-	7.94	-	13.13	-	-	-	-	-
C17	5.64	2.11	1.97	4.85	4.16	5.41	7.25	-	-	-	-	-	-	6.50	8.36
G18	5.96	2.78	2.63	4.97	4.32	-	-	7.98	-	12.83	-	-	-	-	-
T19	5.60	2.36	2.01	4.86	4.13	-	7.18		1.29		-	-	13.54	-	-
A20	6.02	2.90	2.70	5.03	4.39	-	8.17		-	-	6.40	7.30	-	-	-
G21	5.74	2.48	2.02	4.98	4.17	-		7.64	-	12.75	-	-	-	-	-
C22	5.63	2.26	1.99	4.87	4.15	5.25	7.61		-	-	-	-	-	6.33	8.16
A23	6.24	2.92	2.65	5.05	4.35	-		8.28	-	-	6.30	7.70	-	-	-
T24	5.73	2.41	2.00	4.88	4.13	-	7.12	-	1.31		-	-	13.44	-	-
G25	5.83	2.76	2.66	4.98	4.36		-	7.86	-	12.60	-	-	-	-	-
C26	5.78	2.24	2.02	4.84	4.18	5.32	7.34	-	-	-	-	-	-	6.44	8.30
G27	5.97	2.73	2.62	4.80	4.13	-	-	7.74	-	13.08	-	-	-	-	-
C28	5.79	2.23	1.95	4.84	4.19	5.31	7.53	-	-	-	-	-	-	-	-

Table S2. Distance Restraints used for NMR structure calculation of GG28.

NOE contacts	**Strong (1.8-3.0) Å**	**Medium (2.5-4.0) Å**	**Weak (3.5-5.0) Å**	**Watson-Crick (1.8-3.0) Å**
Aromatic-Aromatic	12	11	26	62
Aromatic-Anomeric	78	78	109	
Exchangeable contacts	0	24	17	
Total NOE	90	113	152	
Total Distance Constraints				*417*

TABLE S3. Torsion angles and pseudo phase angle restraints used for NMR structure calculation of GG28.

Torsion angle	NO(TOTAL=164)	LOWER LIMIT(°)	UPPER LIMIT(°)
γ	28	20	100
δ	28	110	170
ε	27	140	220
ζ	27	260	340
α	27	260	340
β	27	140	220
PPA	28	135	185
Total	***192***		

Table S4. The gamma (γ) and epsilon (ε) value of oligonucleotide in free GG28 and and GG28-IR13 complex. Striking disfferences are highlighted.

Residue	γ		ε	
	GG28	GG28+IR13	GG28	GG28+IR13
C2	55.1	-174.4	-174.3	-160.1
G3	49.7	47.2	-177.2	166.1
C4	57.8	49.1	-173.6	-164.0
A5	49.7	-177.3	-179.7	-154.1
T6	60.0	-158.9	-175.0	165.7
G7	58.9	39.0	171.4	173.1
C8	54.8	59.9	-176.3	175.5
T9	53.3	53.7	-171.2	-172.5
A10	54.1	33.6	174.3	-177.7
C11	58.8	53.7	-174.1	173.3
G12	49.0	64.3	-177.5	177.6
C13	55.7	42.0	177.3	153.4
G16	55.4	34.5	174.3	-74.3
C17	56.1	67.4	-175.2	-168.3
G18	50.7	55.2	-178.0	-163.4
T19	58.5	46.3	-174.5	-176.1
A20	54.7	41.1	173.7	-159.6
G21	54.7	51.2	-179.2	-156.0
C22	53.4	42.6	-173.3	-163.2
A23	54.3	56.8	174.9	179.3
T24	58.1	80.2	-175.8	-153.2
G25	54.2	48.6	-178.9	-78.1
C26	53.6	35.4	-178.7	178.0
G27	53.1	56.1	177.3	-172.9

Table S5. Thermodynamics parameters derived using van't Hoff equation from CD melting curve.

DNA	DNA+ Peptide	T_m (^oC)	T_m (K)	ΔH (kcal.mol^{-1})	ΔS (cal.mol^{-1}K^{-1})	ΔG (kcal.mol^{-1})
GG28	GG28	52.2 ± 0.7	325.2	-22.0	-43.4	-9.1
	GG28 + IR13	63.2 ± 0.7	336.2	-31.4	-69.2	-10.8
	GG28+IR13AA	54.5 ± 1.1	327.5	-23.3	-47.1	-9.3
	GG28+IR13HH	56.4± 0.8	329.4	-24.0	-48.6	-9.5
	GG28+IR13FF	55.5± 1.0	328.5	-23.6	-47.6	-9.4
GC28	GC28	40.1 ± 1.2	313.1	-21.7	-45.0	-8.3
	GC28+IR13	50.6 ± 0.7	323.6	-24.4	-51.1	-9.2

Scheme

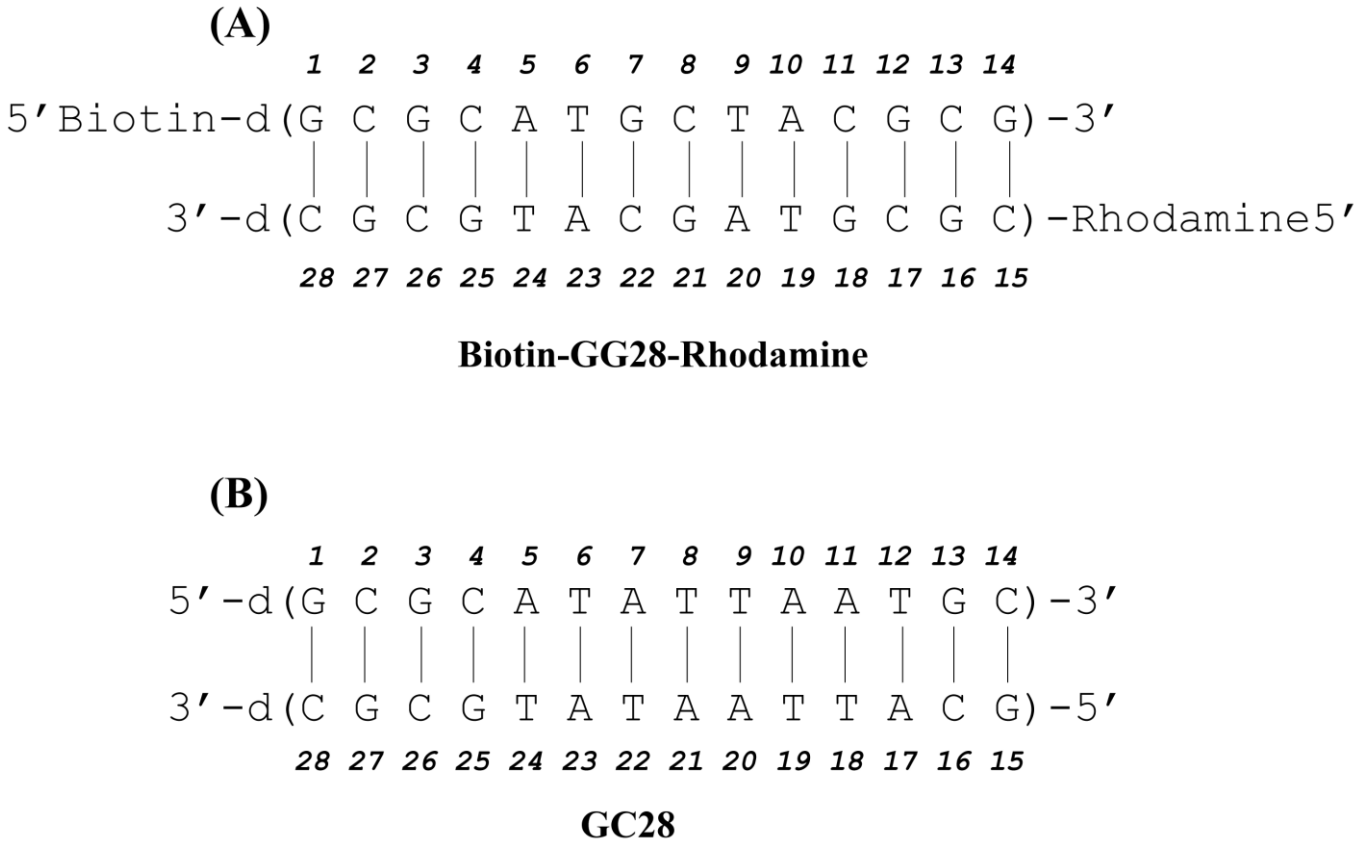

Scheme S1: (A) Sequence of Biotin and Rhodamine labelled GG28. (B) Sequence of GC28.

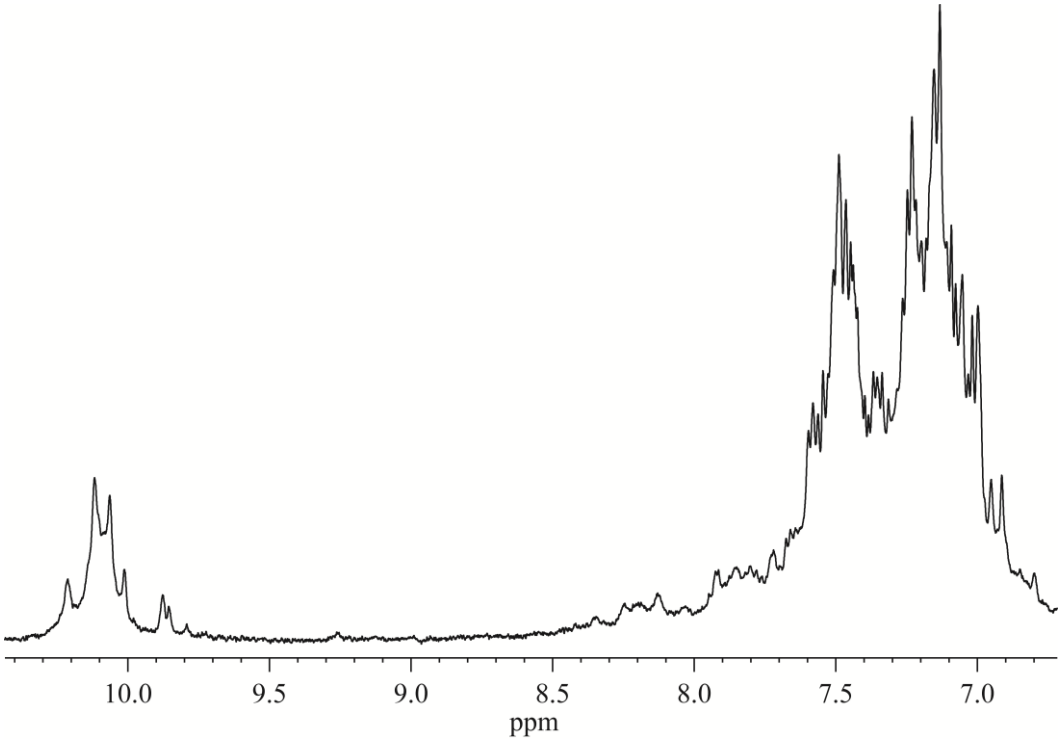

Figure S1: Low field region of the one-dimensional proton NMR spectra of 1 mM indolicidin (20 mM sodium phosphate buffer, pH 7.2 containing 1 mM EDTA and 50 mMNaCl) at 500 MHz and at 25℃. The line broadening of the amide peaks as well as the indole ring protons of Trp clearly indicates that the indolicidin aggregates in the solution.

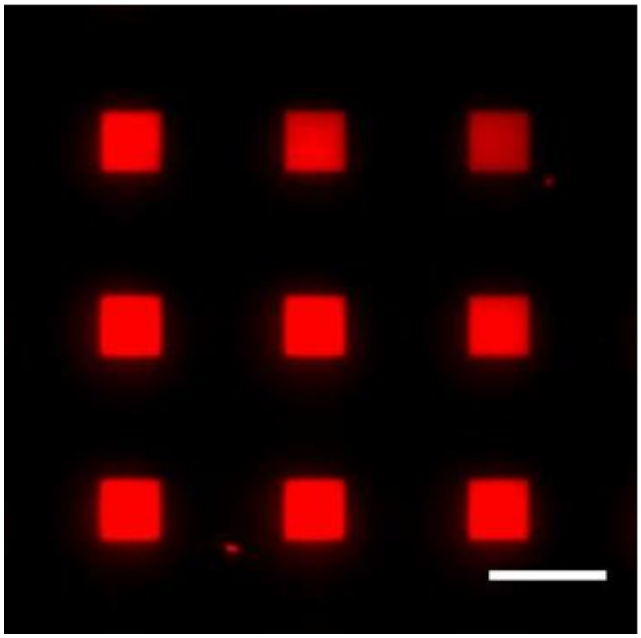

Figure S2: Immobilisation of Biotin-Rhodamine DNA on biotin micropatterned surface through biotin-neutravidin-biotin interaction. Scale bar corresponds to 10 µm.

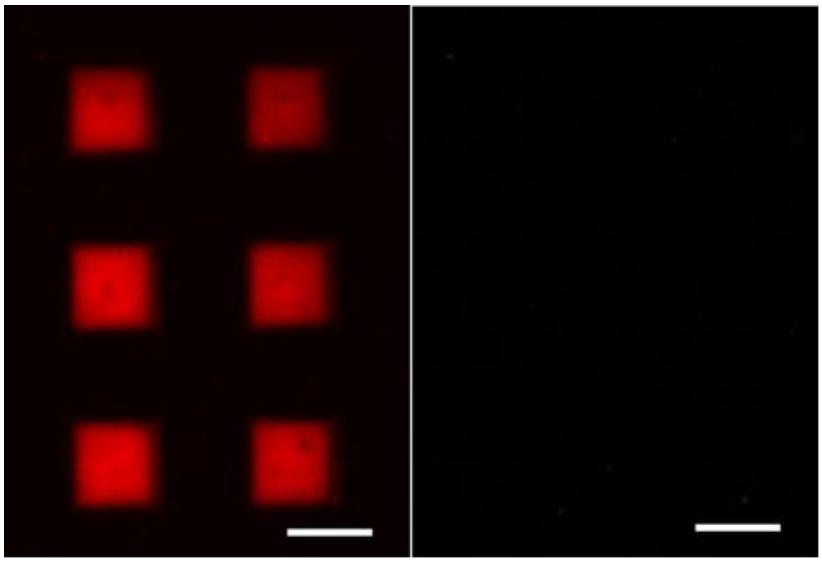

Figure S3: (a) Immobilisation of Avidin-Rhodamine dye on biotin micropatterned surface through avidin-biotin interaction. (b) Absence of green coloured, micropatterned surface indicates that the FITC-IR13 peptide does not bind to biotin micropatterned surface. Scale bar corresponds to 10 µm.

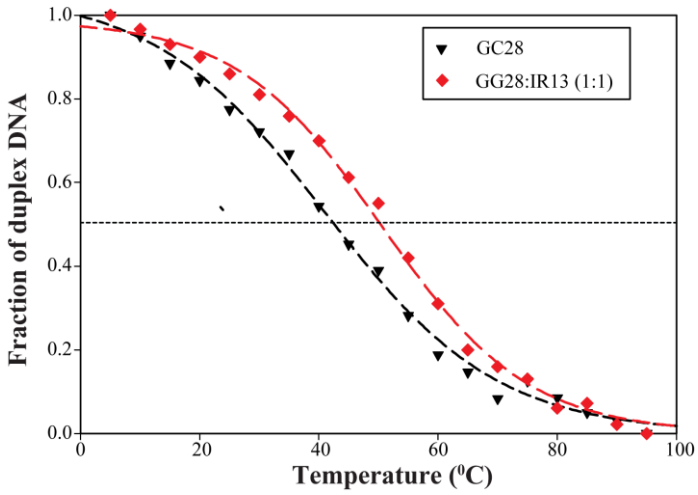

Figure S4: CD melting of GC28 (black colour) in the absence as well as in the presence of IR13 (red colour).

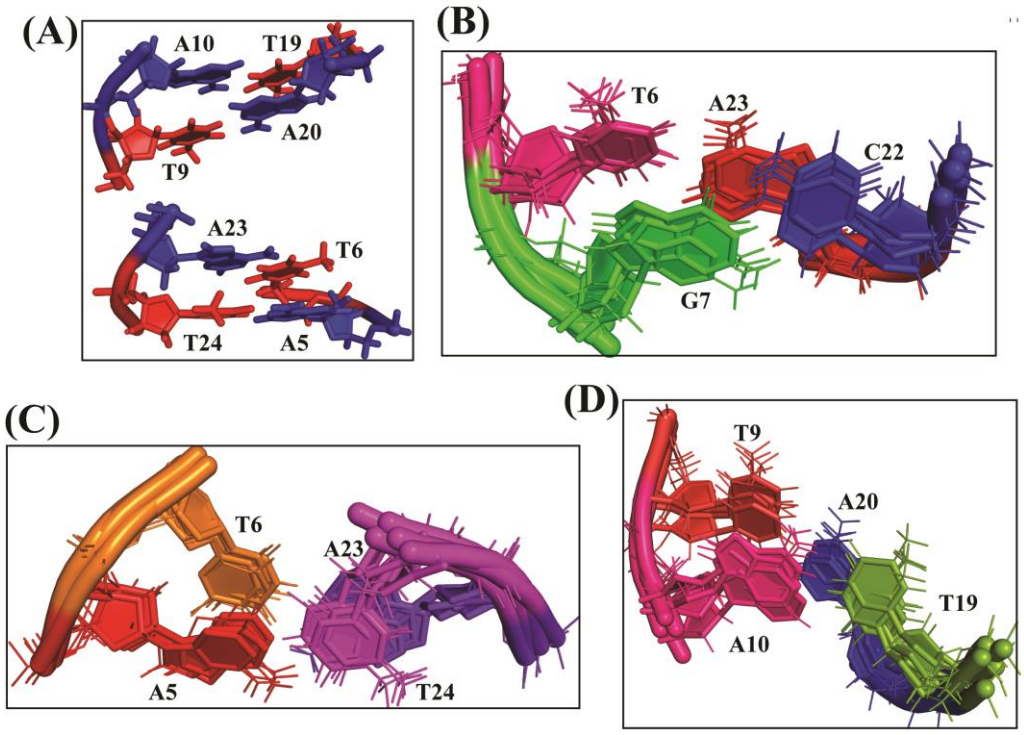

Figure S5: (A) Selected regions of NMR constrained DNA duplex structure of DNA base pairs: A5-T24; T6-A23; T9-A20 and A10-T19. MD ensemble structures of base pairs (B) T6-A23; G7-C22; (C) T6-A23; A5-T24; (D) T9-A20 and A10-T19. All the A-T base pairs are highly dynamic whereas G-C base pairs are conserved.

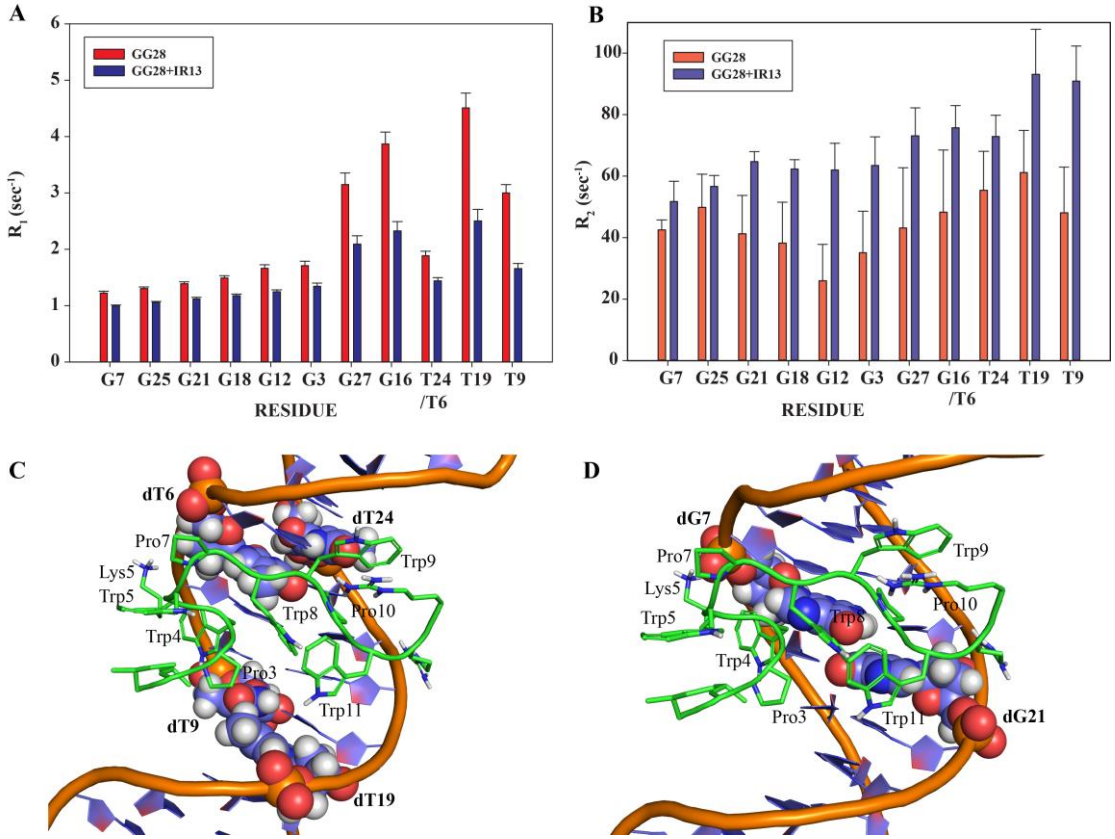

Figure S6: Bar diagrams summarizing imino proton relaxation parameters of the free (Red) and IR13 bound GG28 (blue). (Upper panel) (A) Longitudinal relaxation rates (R_1), (B) transverse relaxation rates (R_2). (Lower panel) Space filling model showing close proximity of (C) T6, T9, T19, T24 and (D) G7, G21of GG28 with IR13. All the Thymine bases are highly affected by strong hydrophobic or stacking interaction between aromatic rings of IR13 and Thymine rings.

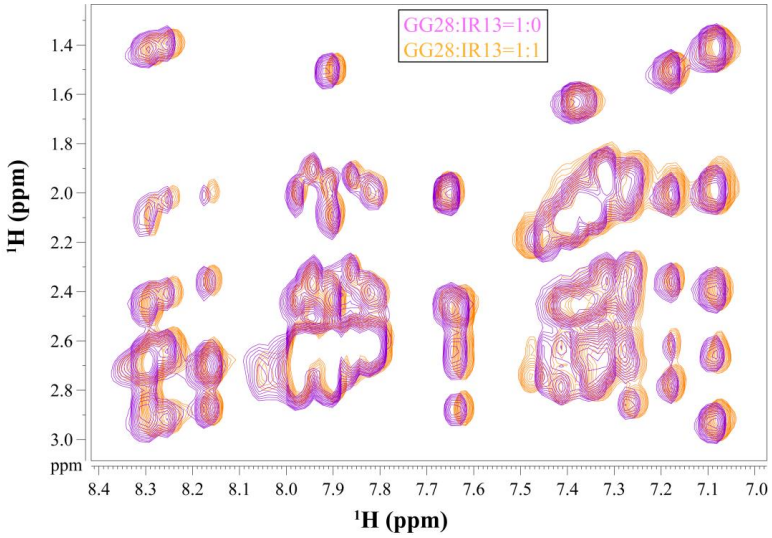

Figure S7: Two dimensional selected ^{1}H-^{1}H NOESY spectra of GG28 (purple) and in complex with IR13 (orange) at 500 MHz, 25℃ and at 150 ms mixing time. Both the spectra are isochronous, indicating that the backbone conformations of GG28 are not changed in the presence of IR13.

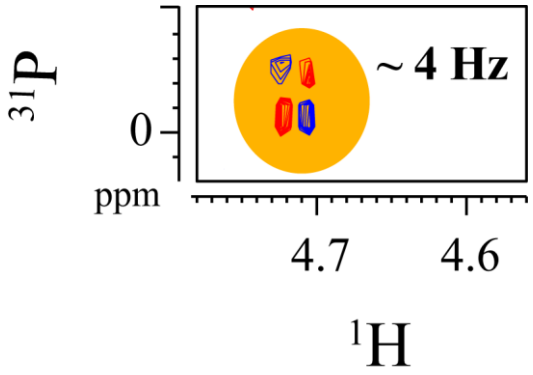

Figure S8: 1H-31P correlation spectrum of GG28, showing the correlation between 3'-5' phosphorus with H5'/H5" and H3' which leads to inform that the γ and ξ dihedral exists in + and *trans* conformations, respectively.

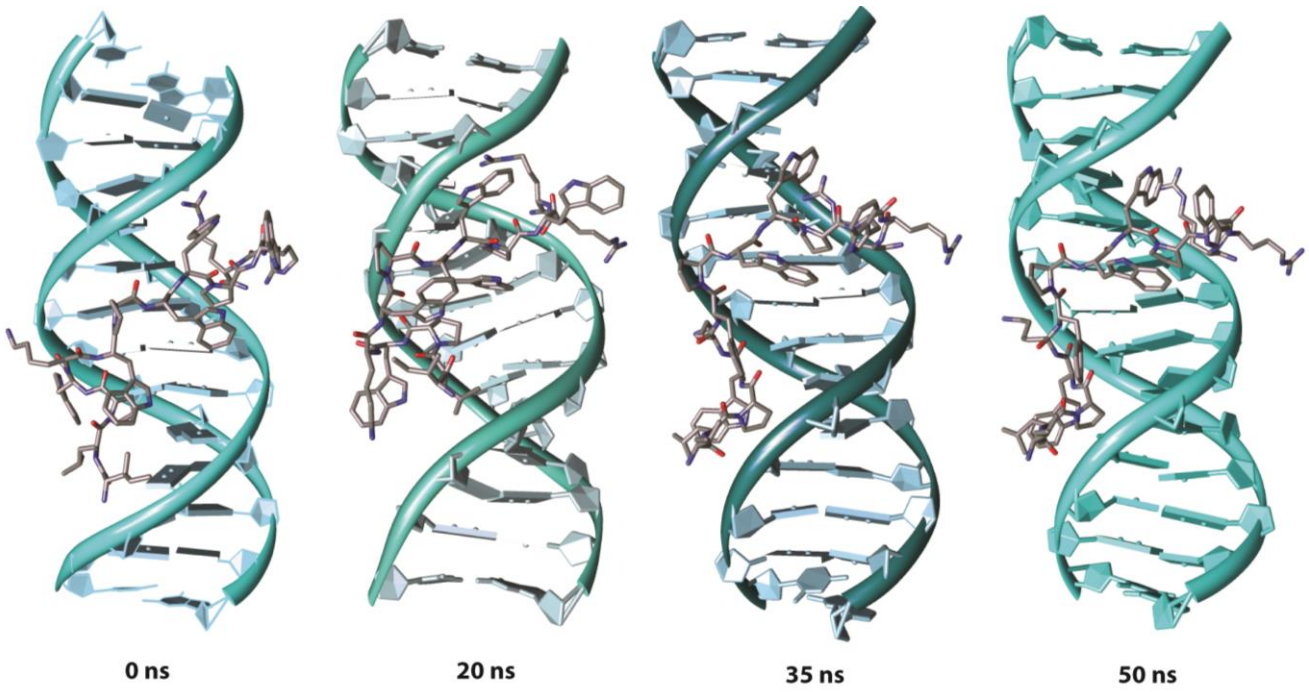

Figure S9: Representation of GG28-IR13 complex from different snapshots of MD simulation time scale. The B-type DNA structure retains throughout the 50ns MD simulation comfirming the in-vitro CD studies of DNA at its complexed state. These images were produced using UCSF Chimera.

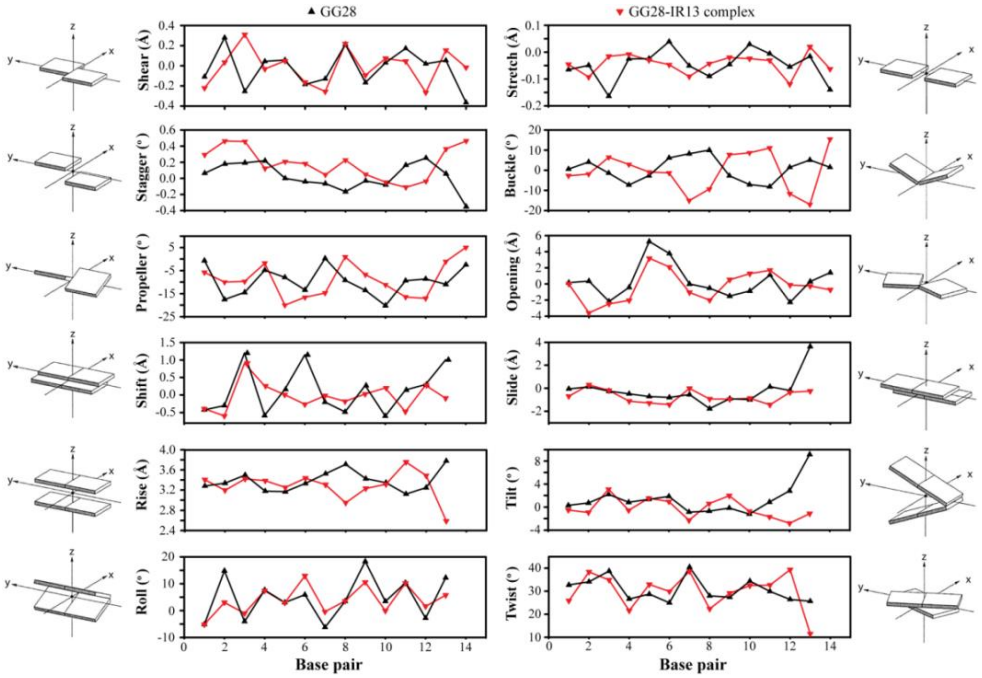

Figure S10: Comparison of the helical parameters for the ensemble of ten structures obtained for control DNA duplex, GG28 and the GG28-IR13 complex. The parameters were calculated using X3DNA program. X3DNA analysis mines out that the base pairing breathing parameters of the complex DNA remains almost in the same domain conferred by the free control DNA.

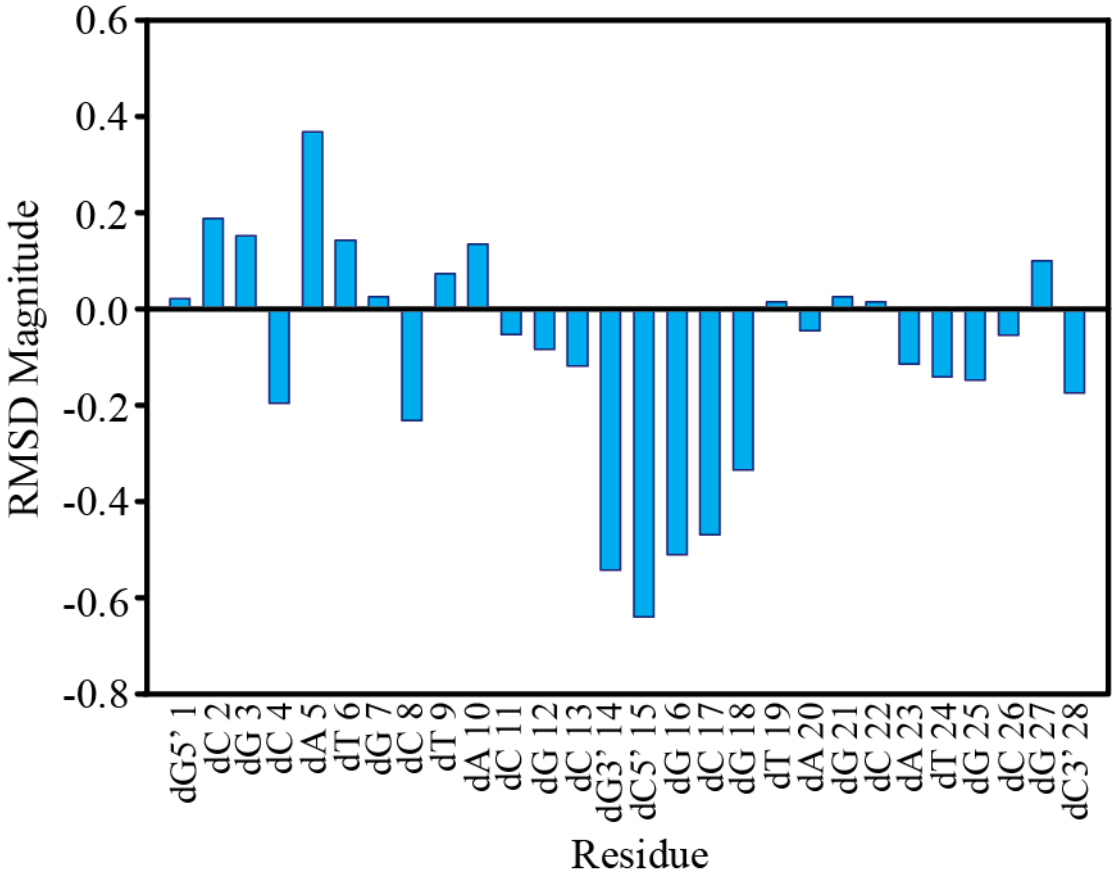

Figure S11: Average rmsd of DNA base from 50 ns MD simulation of NMR restraint derived GG28 and GG28-IR13 complex. The bar diagram of average rmsd represents the magnitude of deviation of all DNA bases in GG28-IR13 complex with reference to GG28.

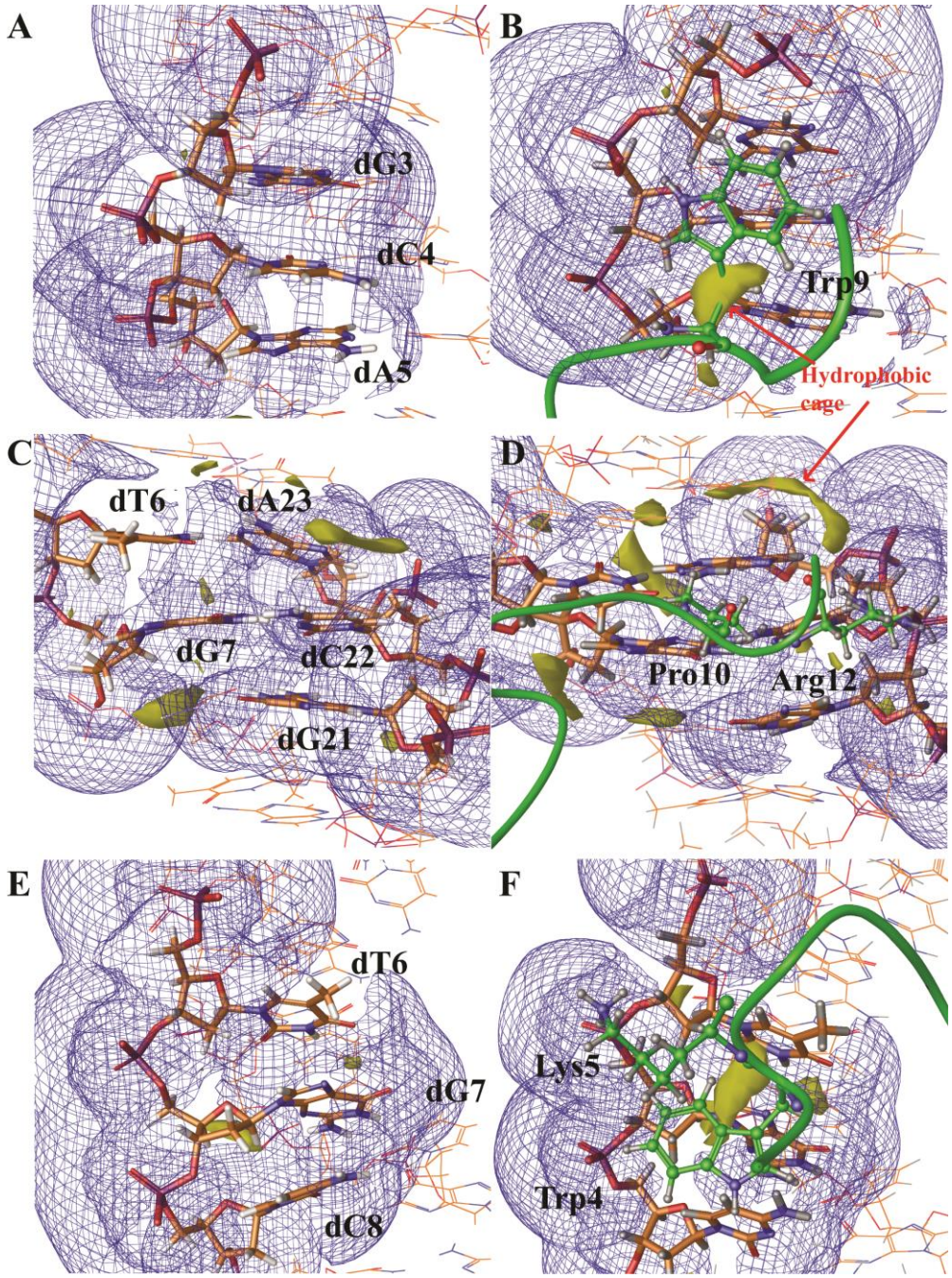

Figure S12: A diagrammatic comparison of the hydrophobic region induced by IR13 residues responsible for desolvation of nucleo-bases. All snapshot were collected after 50 ns MD simulation. The hydrophilic/hydrophobic maps were calculated using *hpp map* in Schrödinger, LLC. The nucleotides of interest were selected and placed inside a grid of 3Å for the calculation of solvation effect. The hydrophilic regions are shown by blue mesh and hydrophobic maps are shown by yellow contours. Corresponding residues of IR13 responsible for desolvation are represented in ball and stick model. (A) Hydrophobic/hydrophilic map (*hpp*) in the region of DNA base: G3, C4 and A5. (B) Hydrophobic region induced by the presence of Trp9. (C) *HPP* map in the region of T6:A23, G7:C22 and G21. (D) Hydrophobic region induced by the presence of Pro10 and Arg12. (E) *HPP* map in region of T6, G7 and C8. (F) Hydrophobic region induced by the presence of Lys5 and Trp4. These images were produced using Schrödinger (Maestro) LLC.

4. References:

[1] W. C. Chan, P. D. White, *Fmoc solid phase peptide synthesis*, Oxford University Press, **2000**.

[2] J. R. Lakowicz, *Principles of fluorescence spectroscopy*, Springer, **2007**.

[3] S. K. Kim, S. Eriksson, M. Kubista, B. Norden, *J. Am. Chem. Soc.* **1993**, *115*, 3441-3447.

[4] S. K. Kim, B. Nordén, *FEBS lett.* **1993**, *315*, 61-64.

[5] a) J. Piehler, A. Brecht, R. Valiokas, B. Liedberg, G. Gauglitz, *Biosens. Bioelectron.* **2000**, *15*, 473-481; b) M. Bhagawati, S. Ghosh, A. Reichel, K. Froehner, T. Surrey, J. Piehler, *Angew. Chem. Int. Ed.* **2009**, *48*, 9188-9191; c) A. Biswas, A. Saha, B. Jana, P. Kurkute, G. Mondal, S. Ghosh, *ChemBioChem* **2013**, *14*, 689-694; d) P. Bieling, L. Laan, H. Schek, E. L. Munteanu, L. Sandblad, M. Dogterom, D. Brunner, T. Surrey, *Nature* **2007**, *450*, 1100-1105.

[6] V. A. Bloomfield, D. M. Crothers, I. Tinoco, *Nucleic acids: structures, properties, and functions*, University science books, **2000**.

[7] a) J.-L. Mergny, L. Lacroix, *Oligonucleotides* **2003**, *13*, 515-537; b) K. J. Breslauer, in *Protocols for Oligonucleotide Conjugates*, Springer, **1994**, pp. 347-372.

[8] a) D. Davis, M. Perlman, R. London, *J. Magn. Reson. Ser. B* **1994**, *104*, 266-275; b) C. Deverell, R. Morgan, J. Strange, *Mol. Phys.* **1970**, *18*, 553-559; c) A. Palmer 3rd, C. D. Kroenke, J. P. Loria, *Methods Enzymol.* **2000**, *339*, 204-238.

[9] D. e. Case, T. Darden, T. Cheatham Iii, C. Simmerling, J. Wang, R. Duke, R. Luo, R. Walker, W. Zhang, K. Merz, *University of California, San Francisco* **2010**, *142*.

[10] V. Hornak, R. Abel, A. Okur, B. Strockbine, A. Roitberg, C. Simmerling, *Proteins* **2006**, *65*, 712-725.

[11] G. Zheng, X.-J. Lu, W. K. Olson, *Nucleic Acids Res.* **2009**, *37*, W240-W246.

[12] A. Rozek, C. L. Friedrich, R. E. Hancock, *Biochemistry* **2000**, *39*, 15765-15774.

[13] D. W. Ritchie, V. Venkatraman, *Bioinformatics* **2010**, *26*, 2398-2405.

[14] W. L. Jorgensen, J. Chandrasekhar, J. D. Madura, R. W. Impey, M. L. Klein, *J. Chem. Phys.* **1983**, *79*, 926-935.

[15] A. Branka, *Phys. Rev. E* **2000**, *61*, 4769-4773.

[16] U. Essmann, L. Perera, M. L. Berkowitz, T. Darden, H. Lee, L. G. Pedersen, *J. Chem. Phys.* **1995**, *103*, 8577-8593.

[17] V. Kräutler, W. F. van Gunsteren, P. H. Hünenberger, *J. Comput. Chem.* **2001**, *22*, 501-508.